Title

Hourly water-carbon interactions modulate decadal water-use efficiency trends inferred from ecosystem-scale measurements

Authors
Chang, Kuang-Yu
Riley, William J
Keenan, Trevor F

Publication Date
2022-11-01

DOI
10.1016/j.agrformet.2022.109158

Hourly water-carbon interactions modulate decadal water-use efficiency trends inferred from ecosystem-scale measurements

Kuang-Yu Chang*,

Climate and Ecosystem Sciences Division, Lawrence Berkeley National Laboratory, Berkeley, CA 94720, USA

William J. Riley,

Climate and Ecosystem Sciences Division, Lawrence Berkeley National Laboratory, Berkeley, CA 94720, USA

Trevor F. Keenan

Climate and Ecosystem Sciences Division, Lawrence Berkeley National Laboratory, Berkeley, CA 94720, USA,

Department of Environmental Science, Policy & Management, UC Berkeley, Berkeley, CA 94720, USA

*Correspondence to: Kuang-Yu Chang, ckychang@lbl.gov

Climate and Ecosystem Sciences Division, Lawrence Berkeley National Laboratory

Berkeley, CA 94720, USA

Phone: (510) 495-8141

Key words: water-use efficiency; carbon cycle; FLUXNET

Abstract

Plant stomatal conductance regulates photosynthesis and transpiration. This physiological link affects ecosystem responses to microclimate and harmonizes carbon, energy, and water exchanges between the biosphere and atmosphere. The relationship between water losses via transpiration and carbon gains via photosynthesis can be quantified by plant water-use efficiency (*WUE*). While leaf- and ecosystem-scale observations both suggest rising *WUE* in recent decades, *WUE* trends inferred from the ecosystem scale are much larger than those inferred from the leaf scale or implied by theory. The unexpectedly large ecosystem-scale *WUE* trends complicate interpretation of ecophysiological responses to changing environmental conditions. Here, we analyze ecosystem-scale *WUE* inferred from 40 FLUXNET sites, each with at least 10 years of measurements. Our results demonstrate that observed ecosystem-scale *WUE* trends are more sensitive to hourly weather conditions than longer-term changes in atmospheric carbon dioxide or vapor pressure deficit. Our analysis shows that Earth System Models participating in CMIP6 did not capture the observed *WUE* sensitivity to inter-site variability and microclimatic conditions. Collectively, our findings suggest that ecosystem-scale *WUE* trends reflect water-carbon interactions across multiple temporal scales, and disentangling factors contributing to emergent ecosystem responses is needed to infer ecophysiological relationships and model structures from observations.

1. Introduction

Terrestrial plants assimilate atmospheric carbon dioxide (CO_2) through photosynthesis, which currently removes about one-third of anthropogenic CO_2 emissions and helps mitigate the rate of climate change (Friedlingstein et al., 2020; Keenan and Williams, 2018). However, plant stomata not only enable CO_2 assimilation, but also lead to water vapor losses via transpiration. This tradeoff is often quantified with a water-use efficiency (*WUE*) metric, for which several different calculation methods have been proposed. For example, *WUE* has been defined as the ratio between carbon assimilation and transpiration at the leaf scale (Driscoll et al., 2020), or as the ratio between gross primary production (GPP) and evapotranspiration (ET) at the ecosystem scale (Bastos et al., 2020). Intrinsic *WUE* (WUE_i) has been defined as the ratio between carbon assimilation and stomatal conductance (GPP and surface conductance at the ecosystem scale) to better represent stomatal controls on plant ecophysiological function (Lloyd et al., 2002; Schulze and Hall, 1982). To account for stomatal responses to vapor pressure deficit (VPD), inherent *WUE* (WUE_{ei}, GPP*VPD*ET^{-1}) (Beer et al., 2009) and underlying *WUE* (*uWUE*, GPP*VPD$^{-0.5}$*ET^{-1}) (Zhou et al., 2014) have been proposed to quantify stomata-mediated carbon and water tradeoffs at the ecosystem scale. All of these *WUE* metrics employ different techniques to quantify different aspects of plant water-carbon interactions (Medlyn et al., 2017).

Importantly, measurements across leaf to ecosystem scales, regardless of the functional forms and sampling methods used to estimate *WUE*, show primarily increasing forest *WUE* over the past several decades (Adams et al., 2020; Guerrieri et al., 2019; Keenan et al., 2013; Mastrotheodoros et al., 2017; Mathias and Thomas, 2021). Studies have attributed the observed *WUE* increases to changes in photosynthesis and/or stomatal conductance driven by rising atmospheric CO_2 concentrations (Guerrieri et al., 2019; Mathias and Thomas, 2021; Ueyama et al., 2020; Walker et al., 2020) and trends in VPD (Yi et al., 2019). Although rising *WUE* trends are qualitatively consistent across spatial scales, *WUE* trends inferred from ecosystem-scale eddy covariance measurements (1.3–2.3% yr^{-1}) (Guerrieri et al., 2019; Keenan et al., 2013; Lavergne et al., 2019; Mastrotheodoros et al., 2017) are much larger than the trends expected with ecophysiological theory (0.5% yr^{-1}) (Mastrotheodoros et al., 2017) and those inferred from carbon isotopes in tree rings (0.2–0.5% yr^{-1}) (Guerrieri et al., 2019; Lavergne et al., 2019; Mathias and Thomas, 2021). Imbalances in energy closure in eddy covariance measurements may contribute to discrepancies between leaf- and ecosystem-scale *WUE* values and trends (Knauer et al., 2018; Wohlfahrt et al., 2009), although the underlying dynamics leading to such discrepancies are under debate (Lavergne et al., 2019; Medlyn et al., 2017; Walker et al., 2020). A potentially overlooked aspect controlling ecosystem-scale *WUE* trends is that annual water and carbon budgets based on eddy covariance methods are sensitive to short-term (hourly - daily) favorable weather conditions that typically cover less than 20% of the observational period (Zscheischler et al., 2016). These factors complicate the interpretation of *WUE* controls inferred from eddy covariance measurements.

Accurate interpretation of observed *WUE* trends is needed to understand biosphere-atmosphere interactions and improve land models used to predict ecosystem structure, function, and services under climate change (Knauer et al., 2017; Yi et al., 2019). While CO_2-induced reductions in stomatal conductance have been proposed to drive the observed *WUE* increases (Keenan et al., 2013), such a physiological response may only be present in species that experienced moisture limitations (Guerrieri et al., 2019). In addition, studies have reported negative *WUE* trends under rising atmospheric CO_2 concentrations (Guerrieri et al., 2019; Knauer et al., 2018), which further suggests that factors other than CO_2 contribute to the observed *WUE* trends. It is therefore important to carefully translate mechanisms inferred from observations to land-model process representations because carbon cycling is strongly impacted by multiple interacting climate-change drivers (Reich et al., 2020).

Here, we investigated factors modulating emergent *WUE* trends inferred from ecosystem-scale flux measurements using the global FLUXNET2015 CC-BY-4.0 Dataset (Pastorello et al., 2020). We hypothesized that changes in short-term water-carbon interactions affect seasonal ecosystem-scale *WUE* estimates and thereby contribute to discrepancies between previously-inferred leaf- and ecosystem-scale *WUE* trends. The FLUXNET2015 database provides half-hourly to hourly ecosystem-scale eddy covariance flux measurements from 212 sites (1532 site-years) across the globe, from which we included sites with at least 10 years of measurements. These criteria resulted in observations from 560 site-years across 40 FLUXNET sites in six ecosystem types: deciduous broadleaf forests, evergreen broadleaf forests, evergreen needleleaf forests, grasslands, mixed forests, and woody savannas (Supplemental Fig. 1 and Supplemental Table 1). For conciseness, we focus our discussion on results inferred from *uWUE* for its better representation of ecosystem-scale carbon and water interactions (Zhou et al., 2014), and report consistent results using WUE_{ei} in the Supplemental Material.

2. Methods

2.1 FLUXNET2015 Dataset

We used half-hourly and hourly temperature (air and soil), precipitation, VPD, solar radiation, net radiation, wind speed, friction velocity (u^*), atmospheric CO_2 concentration, soil water content, latent heat flux, ground heat flux, GPP, photosynthetic photon flux density, and ecosystem respiration data recorded in the FLUXNET2015 CC-BY-4.0 Dataset (http://fluxnet.fluxdata.org/data/fluxnet2015-dataset/). These data were processed following a consistent and uniform processing pipeline (Pastorello et al., 2020).

2.2 Flux data processing

We evaluated *uWUE* and WUE_{ei} for 40 FLUXNET sites of the total of 212 sites in the FLUXNET2015 CC-BY-4.0 Dataset (Supplemental Table 1), where at least 10 years of measurements are available. Wetland and cropland systems were excluded in our analysis to reduce uncertainty caused by water management. Measurements collected during growing season (above-zero air temperature and GPP) and summer (June to August in the Northern Hemisphere and December to February in the Southern Hemisphere) were analyzed and reported.

Following the data processing criteria applied in Mastrotheodoros *et al.* 2017, we excluded negative evapotranspiration, GPP, and VPD values and calculated hourly *uWUE* and WUE_{ei} with daytime measurements (without gap filled data) when incoming shortwave radiation was greater than 100 W m^{-2}. Data extracted during rainy days (defined as days with daily precipitation larger than 1 mm) and 1 day after every rainy day were excluded from the baseline analysis to reduce the influence of ground and canopy evaporation on evapotranspiration. However, a substantial part of the measured evapotranspiration can be attributed to ground and canopy evaporation long after precipitation events (Nelson et al., 2020), affecting the interpretation of transpiration. Therefore, we also examined the sensitivity of our data sampling criteria by (1) screening out data within 5 days of a rain event and (2) including data during and after rainy days.

2. 3 Underlying water-use efficiency calculation

The *uWUE* is defined as the ratio of GPP to ecosystem ET, adjusted for atmospheric evaporative demand represented as the square root of VPD (Zhou et al., 2014). We used two metrics to represent site-year specific *uWUE* during daytime hours described in Section 2.2: (1) the median of site-year specific half-hourly to hourly *uWUE* values ($uWUE_{median}$) and (2) using seasonal aggregates of GPP, ET, and VPD to calculate *uWUE* for each site-year ($uWUE_{aggregate}$).

For $uWUE_{median}$, we calculated hourly *uWUE* for all available measurements within a given site-year (see Section 2.2), and used the median of hourly *uWUE* values to represent the seasonal *uWUE*. For $uWUE_{aggregate}$, we calculated the ratio of the hourly sums of daytime GPP to ecosystem ET, multiplied by the square root of seasonal mean VPD.

Using median values to represent ecosystem-scale *WUE* is recommended for its weaker sensitivity to extremely low or high values measured at the hourly scale (Mastrotheodoros et al., 2017). We used the median values in this study since our analysis indicated that using mean hourly *uWUE* values (instead of $uWUE_{median}$) to represent seasonal *uWUE* leads to larger differences against the values, trends, and interannual variability inferred from $uWUE_{aggregate}$ (Supplemental Fig. 2).

2.4 Most active hour calculation

The most active hour (*MAH*) metric is defined as the number of hours when the investigated property (e.g., GPP) is above a percentile-based threshold for each site-year (Zscheischler et al., 2016). Inspired by the concept that interannual variability in carbon and water fluxes may be attributed to variations in the positive tail of their hourly flux distributions, we evaluated how variations in higher *WUE* hours affect decadal *WUE* trends inferred from eddy covariance measurements. Specifically, we calculated site-specific annual cumulated active hours when hourly *uWUE* is above the 1st to 99th *uWUE* percentiles recorded at each site over the entire measurement period, i.e.,

$$AH(uWUE_x, year) = \sum_{i=1}^{n} 1_{\{hourly\ uWUE(year) > uWUE_x\}} \quad (1)$$

where *AH* is the active hours, *n* is the number of active hours in a given site-year and $uWUE_x$ is the xth percentile of *uWUE* computed over all years for x between 1 and 99. We note that active hours represent time periods when *uWUE* values inferred from half-hourly to hourly measurements are within the *uWUE* percentiles selected in our calculation. Active hour time series calculated at each *uWUE* percentile were compared with the $uWUE_{median}$ time series at each site to infer the percentile where the average correlation over the 40 FLUXNET sites reached its maximum that defines *MAH*. *MAH* indicates the annual number of hours that strongly affect interannual variability in ecosystem-scale carbon and water fluxes (Zscheischler et al., 2016), and is thus suitable to quantify effects of short-term water-carbon interactions on seasonal *uWUE*. Detailed *MAH* descriptions, including mathematical derivation, can be found in Zscheischler *et al* 2016.

We examined three sets of *MAH* measures to investigate which *uWUE* percentile best explains the decadal $uWUE_{median}$ trends inferred from the 40 Fluxnet sites. Specifically, we evaluated correlations between *MAH* and $uWUE_{median}$ when *MAH* is defined as the number of hours when *uWUE* is above (1) a fixed *uWUE* threshold based on the highest correlation between *MAH* and $uWUE_x$ across the 40 FLUXNET sites ($uWUE_{78}$, when *uWUE* exceeds the 78th percentile of the *uWUE* inferred from all years at a given site); (2) ecosystem-specific *uWUE* based on the highest correlation between *MAH* and $uWUE_x$ inferred from each ecosystem type; and (3) site-specific *uWUE* based on the highest correlation between *MAH* and $uWUE_x$ inferred from each site. For conciseness, we focus our discussion on results inferred from using a fixed *uWUE* threshold ($uWUE_{78}$), and report consistent results using site- and ecosystem-specific *uWUE* thresholds in the Supplemental Material.

2.5 Random-forest model selection

We used random-forest model selection to identify the most important predictors for short-term water-carbon interactions represented by hourly *uWUE*. Individual predictors were ranked and scaled by their permutation importance calculated at the 40 FLUXNET sites. The random-forest model selection was performed by the Statistics and Machine-Learning Toolbox in Matlab (MathWorks Inc., 2019, version 9.7.0).

The permutation importance of ten predictors on *uWUE* was analyzed: VPD, u^*, air and soil temperatures, soil water content, downwelling solar radiation, residual energy imbalance (differences between the sum of net radiation and ground heat flux and the sum of sensible and latent heat fluxes), atmospheric CO_2 concentration, site identity, and ecosystem type. Site identity and ecosystem type were labeled as categorical data and the other eight predictors were labeled as numerical data in our random-forest models. Categorical features in site identity and ecosystem type were assigned by the site name and IGBP (International Geosphere-Biosphere Programme) vegetation classification reported at each FLUXNET site, respectively. *uWUE* values are represented by the median of site-year specific hourly *uWUE* values ($uWUE_{median}$).

To further investigate factors modulating water-carbon interactions under varying weather conditions, we calculated mean climate conditions at individual *uWUE* percentiles recorded at each site-year over the entire measurement period, i.e.,

$$\overline{Predictor_k}(uWUE_x, year) = \frac{1}{n}\sum_{i=1}^{n} Predictor_{k\{uWUE(year)>uWUE_x\}} \quad (2)$$

where $\overline{Predictor_k}$ is the mean climate condition, $Predictor_k$ is the hourly weather condition from observations, n is the number of hours in a given site-year, and $uWUE_x$ is the x^{th} percentile of *uWUE* computed over all years for x between 1 and 99. For each site-year, we evaluated the permutation importance of six climate drivers (VPD, u^*, air and soil temperatures, soil water content, and downwelling solar radiation), residual energy imbalance, and atmospheric CO_2 concentrations on *uWUE* at each *uWUE* percentile.

In addition to the measured atmospheric CO_2 concentrations, we evaluated the decadal CO_2 trends inferred from NOAA's CarbonTracker (version CT2019B, Jacobson et al., 2020) to examine potential bias associated with temporal drifts in long-term CO_2 measurements. Our results indicate that decadal CO_2 trends are comparable between the two datasets (0.49 % yr^{-1} for FLUXNET2015 and 0.53 % yr^{-1} for CarbonTracker), although the measured atmospheric CO_2 concentrations are generally lower than those inferred from CarbonTracker (Supplemental Fig. 3).

2.6 CMIP6 models

We used model outputs from the AMIP experiments released by the Coupled Model Intercomparison Project Phase 6 (CMIP6), where each model was driven by standardized forcings of prescribed CO_2 concentration and sea surface temperature for the years 1979−2014 (Eyring et al., 2016). We analyzed data derived from eight models that provided monthly outputs for GPP, transpiration, relative humidity, and air temperature for *uWUE* calculations. The eight models are CESM2 (Danabasoglu et al., 2020), CanESM5 (Swart et al., 2019), CESM2-WACCM (Danabasoglu et al., 2020), CMCC-CM2-SR5 (Cherchi et al., 2019), IPSL-CM6A-LR (Boucher et al., 2020), GISS-E2-1-G (Kelley et al., 2020), MPI-ESM1-2-HR (Gutjahr et al., 2019), and NorESM2-LM (Seland et al., 2020), with model details provided in Supplemental Table 2. These monthly outputs were extracted at gridcells containing the 40 FLUXNET sites. We note that CMIP6 models were used to evaluate the *WUE* trends captured by existing land surface models, not the water-carbon interaction dynamics embedded in ecosystem process parameterization.

2.7 Statistical Analyses

uWUE trends were estimated using the Mann-Kendall Tau non-parametric trend test with Sen's method using the Matlab (MathWorks Inc., 2019, version 9.7.0) ktaub function (Burkey, 2022). The violin plots, used to present the inferred *uWUE* properties, are generated by the Violin function (Bechtold et al., 2021).

3. Results

3.1 *uWUE* sensitivity to data processing

The growing season *uWUE* values and trends inferred from our study sites differ substantially within and across the examined ecosystem types (Fig. 1a, b), highlighting the need to recognize effects of varying microclimate and ecosystem types on *uWUE* interpretation. As described in Methods, we used two metrics to measure growing season *uWUE* (Section 2.3): (1) $uWUE_{median}$ (based on the median of site-year specific hourly *uWUE* values) and (2) $uWUE_{aggregate}$ (based on the seasonal aggregate of GPP, ET, and VPD). Consistent estimates of growing season *uWUE* values, trends, and interannual variability were inferred from $uWUE_{median}$ and $uWUE_{aggregate}$ (Fig. 1). Our results thus indicate that the distribution of hourly *uWUE* can be used to evaluate how short-term ecosystem responses modulate interannual and multi-year *uWUE* trends while reflecting consistent seasonal dynamics shown in seasonal aggregate approaches.

We found that *uWUE* values, trends, and interannual variability are not sensitive to the presence of wet canopy conditions that include data during and after rainy days

(Supplemental Fig. 4). Consistent *uWUE* values, trends, and interannual variability were found when using data that exclude measurements made within 5 days of a rain event (Supplemental Fig. 5). While we acknowledge that using evapotranspiration observed one day after rain may not be an adequate approximation of transpiration (Nelson et al., 2020), our sensitivity tests suggest that the *uWUE* properties present in this study are not subject to our data processing scheme.

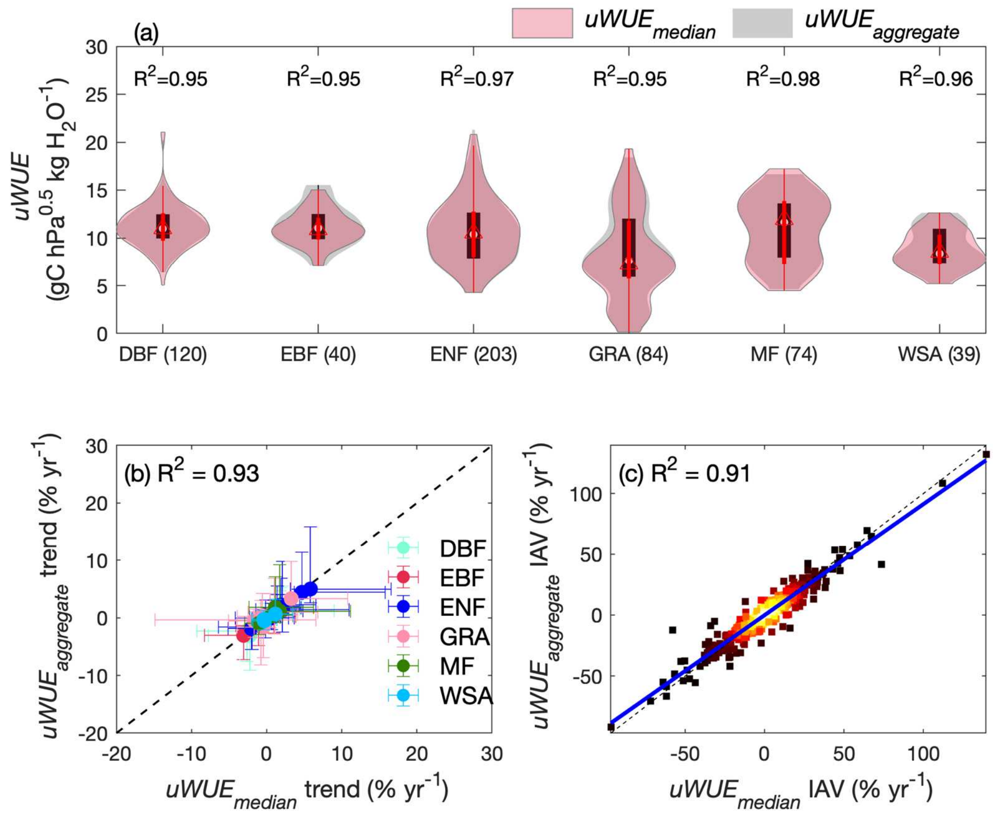

Figure 1. The distribution of seasonal $uWUE_{median}$ and $uWUE_{aggregate}$ values computed at deciduous broadleaf forests (DBF), evergreen broadleaf forests (EBF), evergreen needleleaf forests (ENF), grasslands (GRA), mixed forests (MF), and woody savannas (WAS) (a). The red (black) central mark, and the bottom and top edges of the red (black) box in each violin plot indicate the 50th (median), 25th, and 75th percentiles, respectively,

of $uWUE_{median}$ ($uWUE_{aggregate}$). *uWUE* trends estimated by the Mann-Kendall Tau non-parametric trend test with Sen's method (b). Error bars represent the lower and upper confidence interval for Sen's slope. The comparison between interannual variability in $uWUE_{median}$ and $uWUE_{aggregate}$ (c). Lighter colors in the density scatter plot represent denser data points. Solid blue and dashed black lines represent the linear best-fit and one-to-one lines, respectively. The R^2 values for $uWUE_{median}$ and $uWUE_{aggregate}$ values (a), trends (b), and interannual variability (c) are denoted in the corresponding subplot.

3.2 *uWUE* sensitivity to hourly weather conditions

We calculated the number of active hours when hourly *uWUE* exceeds site-specific *uWUE* thresholds to quantify effects of short-term water-carbon interactions on *uWUE* trends, based on the Most Active Hour (*MAH*, Section 2.4) framework (Zscheischler et al., 2016). Across the 40 FLUXNET sites, correlations between active hour and seasonal *uWUE* generally increase with increasing *uWUE* percentile up to a maximum around the 78th *uWUE* percentile before correlations decrease again (Fig. 2). We thus define *MAH* for each site-year as the number of hours when hourly *uWUE* exceeds the 78th percentile of the *uWUE* inferred from all years at a given site. Consistent results were found with *uWUE* and WUE_{ei} inferred from measurements taken at different seasons (growing season vs. summer) and canopy conditions (wet vs. dry), where *MAH* is defined as the number of hours when site-specific *WUE* exceeds its 70th to 83rd percentiles (Supplemental Figs. 6, 7, 8, 9). These results indicate that temporal variations in annual *WUE* are more sensitive to frequency changes in high *WUE* events (i.e., annual hours when $WUE \geq WUE_{78th}$) than gradual shifts in baseline WUE (i.e., around WUE_{50th}) under a changing climate.

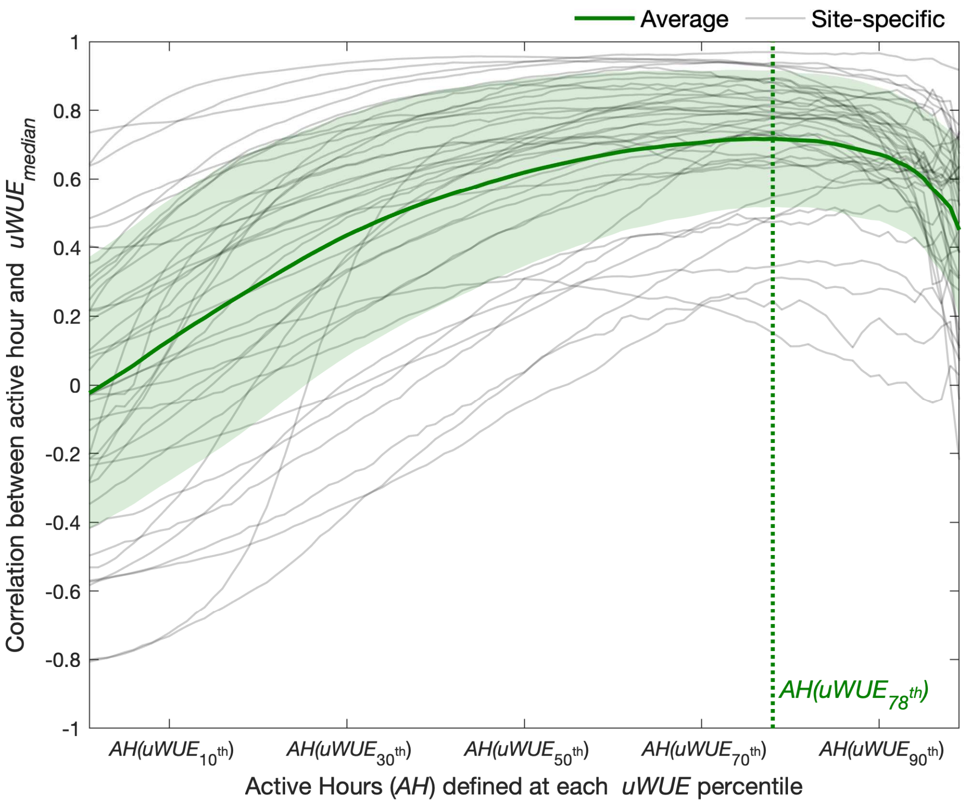

Figure 2. The correlation between active hour and $uWUE_{median}$ time series. The green solid line and shaded area represent the average correlation between active hour (*AH*) and $uWUE_{median}$ and the corresponding standard deviation among the 40 FLUXNET sites, respectively. Gray solid lines represent results inferred from individual sites. The dashed green line indicates the percentile (78^{th}) resulting in the highest overall correlation between active hour and $uWUE_{median}$ among the 40 FLUXNET sites.

3.3 Factors regulating decadal *uWUE* time series and trends

Our results indicate that temporal variations in *MAH* have stronger predictability on $uWUE_{median}$ than temporal variations in baseline active hours (represented by the number of hours when *uWUE* is within its 40th to 60th percentiles), GPP, ET, VPD, and CO_2 concentrations on decadal timescales (Fig. 3). We did not identify any abrupt breaks in $uWUE_{median}$ and *MAH* time series that could affect the correlation inferred from the 40 FLUXNET sites (Supplemental Figs. 10, 11). Implementing site- or ecosystem-specific *MAH-uWUE* relationships does not substantially improve the correlation between *MAH* and $uWUE_{median}$, supporting our use of a fixed *uWUE* threshold ($uWUE_{78}$) in representing temporal changes in hourly weather conditions (Supplemental Fig. 12).

The relatively weak relationships between $uWUE_{median}$ and any single ecophysiological factor (i.e., GPP, ET, VPD, and CO_2 concentrations) indicate that variability in ecosystem-scale *WUE* cannot be explained without representing water-carbon interactions. While temporal variations in GPP, ET, VPD, and CO_2 concentrations correlate well with $uWUE_{median}$ at some of the sites, they do not individually explain variability in $uWUE_{median}$ across all the examined ecosystems. Although CO_2 concentrations measured at eddy covariance towers may degrade with temporal drifts in CO_2 sensors, the comparable correlation inferred from FLUXNET2015 (0.1 ± 0.4) and CarbonTracker (0.2 ± 0.5) datasets suggest that our analysis is not sensitive to potential biases in CO_2 measurements. Consistent results were also found with the inclusion of wet canopy conditions (Supplemental Fig. 13), *uWUE* inferred from summer only measurements (Supplemental Fig. 14), WUE_{ei} inferred from growing season (Supplemental Fig. 15), and WUE_{ei} inferred from summer only measurements (Supplemental Fig. 16).

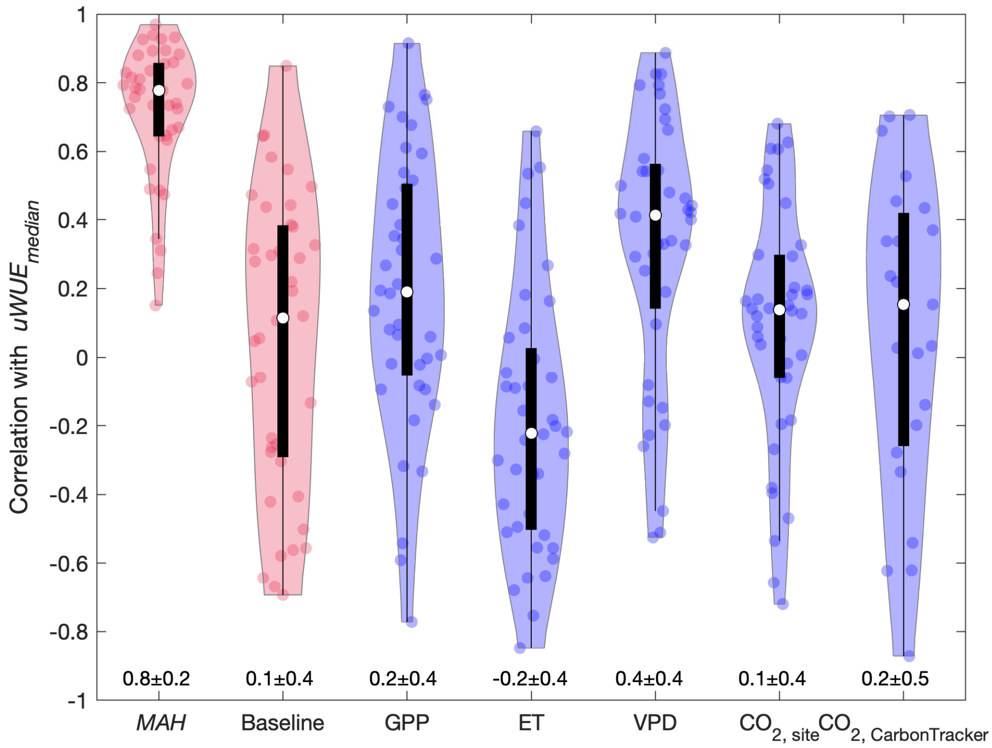

Figure 3. The distribution of correlations between growing season *uWUE*, *MAH*, baseline active hour (Baseline), gross primary productivity (GPP), evapotranspiration (ET), vapor pressure deficit (VPD), FLUXNET2015 CO_2 concentrations ($CO_{2,\ site}$), and CarbonTracker CO_2 concentrations ($CO_{2,\ CarbonTracker}$). The baseline active hour indicates the number of hours when *uWUE* is within its 40th to 60th percentiles. The open circle, bottom edge, and top edge of the black box in each violin plot indicate the 50th (median), and the 25th and 75th percentiles of the inferred correlation values, respectively. Numbers below each violin plot represent the median ± standard deviation of the correlation inferred from the 40 FLUXNET sites.

In terms of decadal trends, we found a strong relationship between *MAH* and $uWUE_{median}$ trends, suggesting *WUE* trends inferred from eddy covariance measurements are modulated by variations in hourly water-carbon interactions that cover less than 22% of the observational period (Fig. 4). Trends in baseline active hour, GPP, ET, VPD, and CO_2 concentrations explain limited variability in $uWUE_{median}$ trends, and their magnitudes do not scale with $uWUE_{median}$ trends. While correlation does not imply causality, our results demonstrate the need to filter out *MAH* effects on ecosystem-scale *WUE* trends to properly interpret observationally-inferred ecophysiological responses across multiple temporal scales.

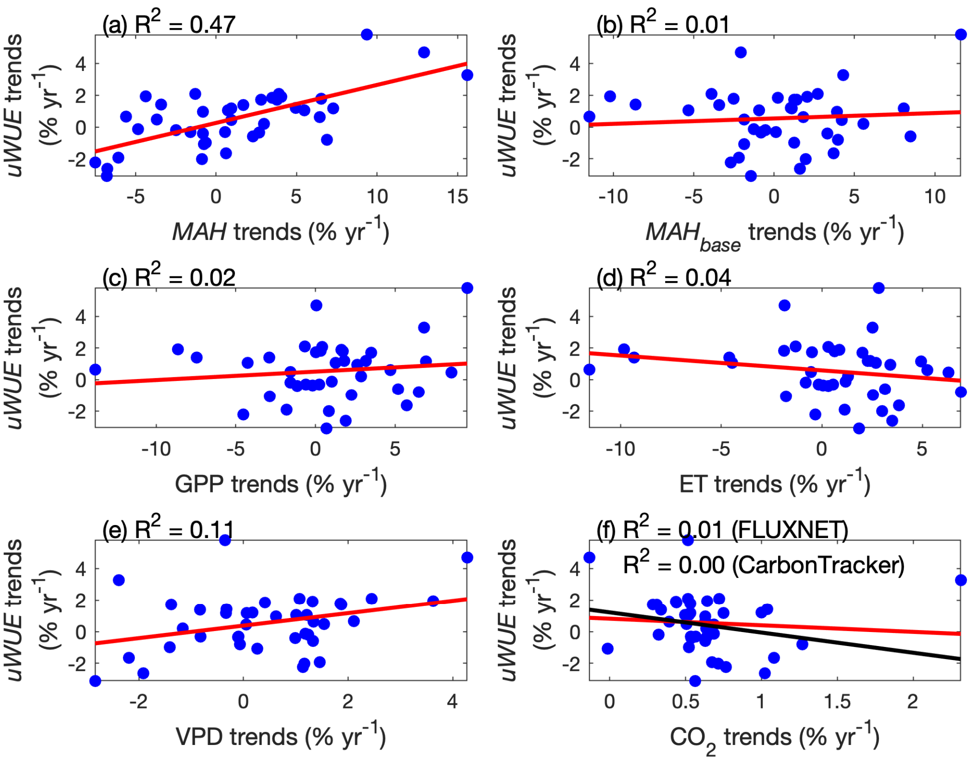

Figure 4. Scatter plots between decadal *uWUE*, *MAH* (a), baseline active hour (b), gross primary productivity (GPP, c), evapotranspiration (ET, d), vapor pressure deficit (VPD, e), and CO_2 concentration (f) trends inferred from the 40 FLUXNET sites. Solid lines are linear regression lines for the scatters examined in each plot.

For the 40 FLUXNET sites, the median $uWUE_{median}$ and $uWUE_{aggregate}$ trends inferred from observations (0.4–0.6% yr^{-1}) are comparable to the median $uWUE_{aggregate}$ trend inferred from CMIP6 simulations (0.3 % yr^{-1}) (Fig. 5a). The magnitude of the observed and simulated decadal *uWUE* trends is comparable to *WUE* trends inferred from leaf-scale observations (0.2–0.5% yr^{-1}) (Guerrieri et al., 2019; Lavergne et al., 2019; Mathias and Thomas, 2021), and is weaker than those from ecosystem-scale observations at forest (0.9–2.3% yr^{-1}) (Guerrieri et al., 2019; Keenan et al., 2013; Lavergne et al., 2019; Mastrotheodoros et al., 2017).

Our results show that *MAH* trends may amplify or dampen the corresponding *uWUE* trends (Fig. 5b), suggesting that ecosystem-scale plant water-carbon interactions depend on microclimatic conditions and are thereby subjective to sampling site selection. For example, sites with positive *MAH* trends experience substantially stronger increases in $uWUE_{median}$ and $uWUE_{aggregate}$ (Fig. 5b; 1.0±1.4 to 1.2±1.7% yr^{-1}) than those with negative *MAH* trends (Fig. 5b; -0.3±1.6 to -0.4±1.6% yr^{-1}). Consistent sensitivities to *MAH* were found with the inclusion of wet canopy conditions (Supplemental Fig. 17) and with the use of WUE_{ei} (Supplemental Fig. 18).

Such *uWUE* (and WUE_{ei}) sensitivity to *MAH* demonstrates the need to recognize effects of short-term water-carbon interactions on the interpretation of decadal ecosystem responses to climate change. The modeled CMIP6 $uWUE_{aggregate}$ trends show substantially lower site-to-site variability than the observed $uWUE_{median}$ and $uWUE_{aggregate}$ trends, and are not sensitive to varying *MAH* trends. Discrepancies between the observed and CMIP6 modeled *uWUE* trends could stem from scale mismatch and incomplete process representations, and should be investigated in future analyses.

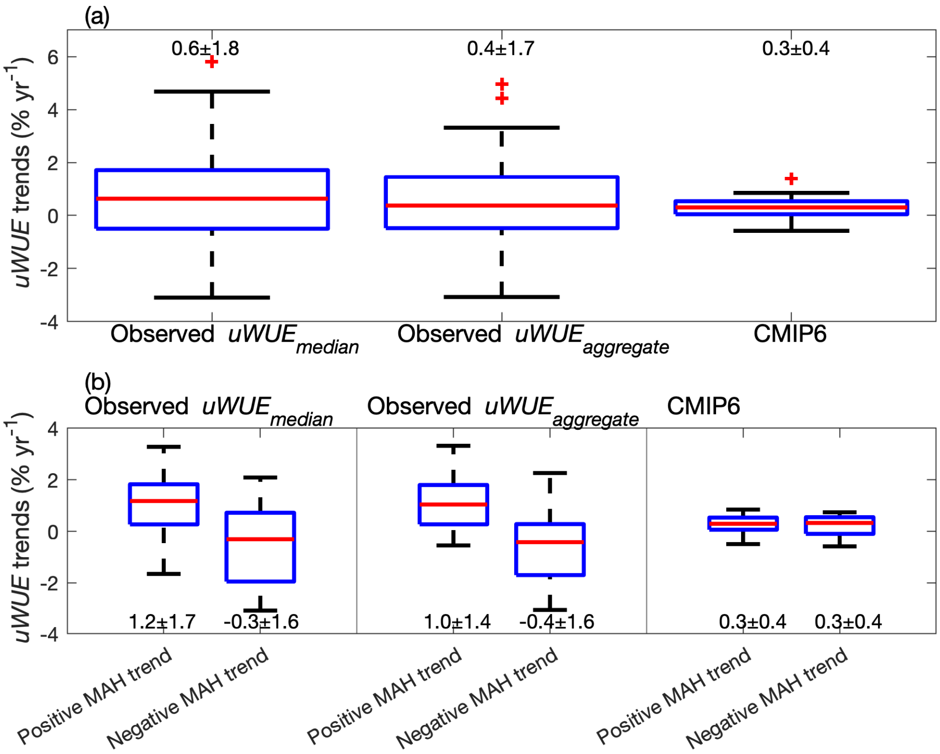

Figure 5. The distribution of trends in $uWUE_{median}$, $uWUE_{aggregate}$, and *uWUE* inferred from CMIP6 models when changes in *MAH* trends are not recognized (a), and explicitly represented (b). The red central mark, and the bottom and top edges of the blue box indicate the median, and the 25th and 75th percentiles, respectively. The black whiskers extend to the most extreme data points not considered outliers denoted in red plus symbol. Numbers above each box plot indicate the median ± standard deviation of the corresponding *uWUE* trend.

3.4 Factors regulating hourly *uWUE*

Our random-forest predictor importance analysis shows large inter-site variability in hourly *uWUE* inferred from the 40 FLUXNET sites, demonstrating that ecosystem-scale water-carbon interactions are site-specific properties that depend on factors other than mean climate conditions (Fig. 6). The large inter-site variability in *uWUE* is not driven by different energy balance closures between sites, as energy closure imbalance is not the dominant factor controlling *uWUE*. The relatively weak *uWUE* sensitivity to ecophysiological factors suggests that observed *uWUE* trends are unlikely attributed to ecosystem responses to temporal variations in any single ecophysiological factor (e.g., VPD or CO_2 concentrations). Our analysis indicates that plant water-carbon interactions inferred from eddy covariance measurements have to be evaluated at a site-to-site basis, even though the inclusion of both inter-site and inter-type variability could diminish the importance of inter-type variability on *uWUE*. Consistent results were found at seasonal timescales with $uWUE_{median}$ and $uWUE_{aggregate}$, highlighting the need to recognize inter-site variability to properly disentangle factors regulating emergent water-carbon interactions (Supplemental Fig. 19). Additionally, our analysis on $uWUE_{median}$ and $uWUE_{aggregate}$ demonstrates that *MAH* is the second most important factor regulating seasonal *uWUE*, which may be attributed to the hourly weather conditions embedded in *MAH* that vary among sites.

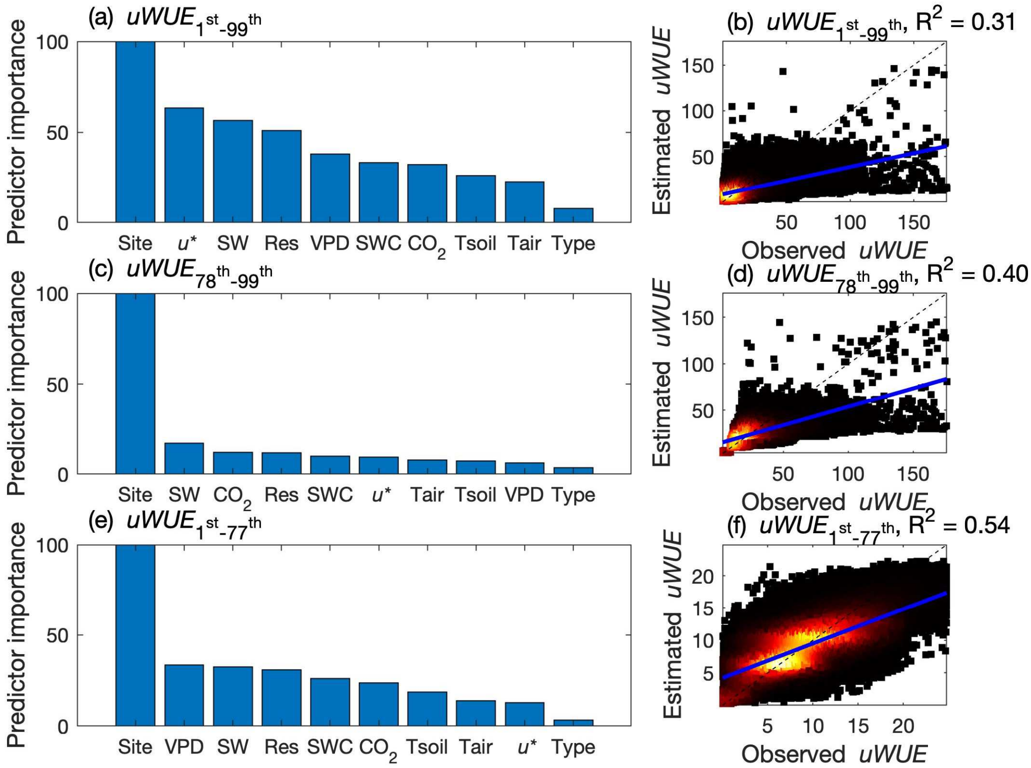

Figure 6. The predictor importance estimated by our random-forest model for the 1st to 99th (a), 78th to 99th (c), and 1st to 77th (e) *uWUE* percentile bins inferred from the 40 FLUXNET sites. Ten ecophysiological factors were compared for their predictor importance on *uWUE*: vapor pressure deficit (VPD), air (Tair) and soil (Tsoil) temperatures, soil water content (SWC), friction velocity (u^*), downwelling solar radiation (SW), residual energy imbalance (Res), atmospheric CO_2 concentration, site identity (Site), and ecosystem type (Type). Site and Type are categorical data that represent effects of undetected variables at a given ecosystem and ecosystem type, respectively. The performance of the *uWUE* percentile bins estimated for the 1st to 99th (b), 78th to 99th (d), and 1st to 77th (f) percentiles. Lighter colors in the density scatter

plot represent denser data points. Solid blue and dashed black lines represent the linear best-fit and one-to-one lines, respectively.

Because of the large inter-site variability (Fig. 6), we built site-specific random-forest models to evaluate factors regulating water-carbon interactions under hourly weather conditions labeled as *MAH* (i.e., times when *uWUE* exceeds its 78th percentile). Our results indicate that hourly *uWUE* is strongly affected by variations in solar radiation across the 40 FLUXNET sites (Fig. 7a, b), suggesting that emergent water-carbon interactions depend on ecosystem responses to radiative energy input. Measurements collected from the 78th to 99th *uWUE* percentiles also indicate that solar radiation is the most important predictor for *uWUE* (Fig. 7c, d), reinforcing the need to recognize effects of canopy radiative transfer on the interpretation of *uWUE* values and trends. On the other hand, lower *uWUE* values (i.e., $uWUE < uWUE_{78th}$) are sensitive to variations in multiple ecophysiological factors (Fig. 7e, f), instead of being driven by a single dominant controller across the 40 FLUXNET sites.

Differences in predictor importance inferred from different *uWUE* percentile intervals suggest that higher *uWUE* is driven by both enhanced feedbacks to solar radiation and adjustments to changing ecophysiological factors. Such shifts in ecosystem responses are likely associated with changes in hourly weather conditions that integrate the examined ecophysiological effects on emergent water-carbon interactions. Since *MAH* quantifies the number of hours when solar radiation becomes the most important predictor controlling the elevated *uWUE*, temporal variations in *MAH* contributes to *uWUE* variability that correlates with decadal *uWUE* trends. Our results show that water-carbon interactions inferred from eddy covariance measurements are modulated by ecosystem responses to hourly weather conditions that may be independent of decadal trends in ecophysiological factors. The strong effects of hourly ecosystem processes suggest that variations in canopy scalar profiles and turbulent mixing rates may contribute to discrepancies between *WUE* trends previously-inferred from leaf- and ecosystem- scale observations. The *MAH* metric presented here could help filter out non-physiological effects on water-carbon interactions inferred from eddy covariance measurements to better represent ecosystem responses to long-term climate change.

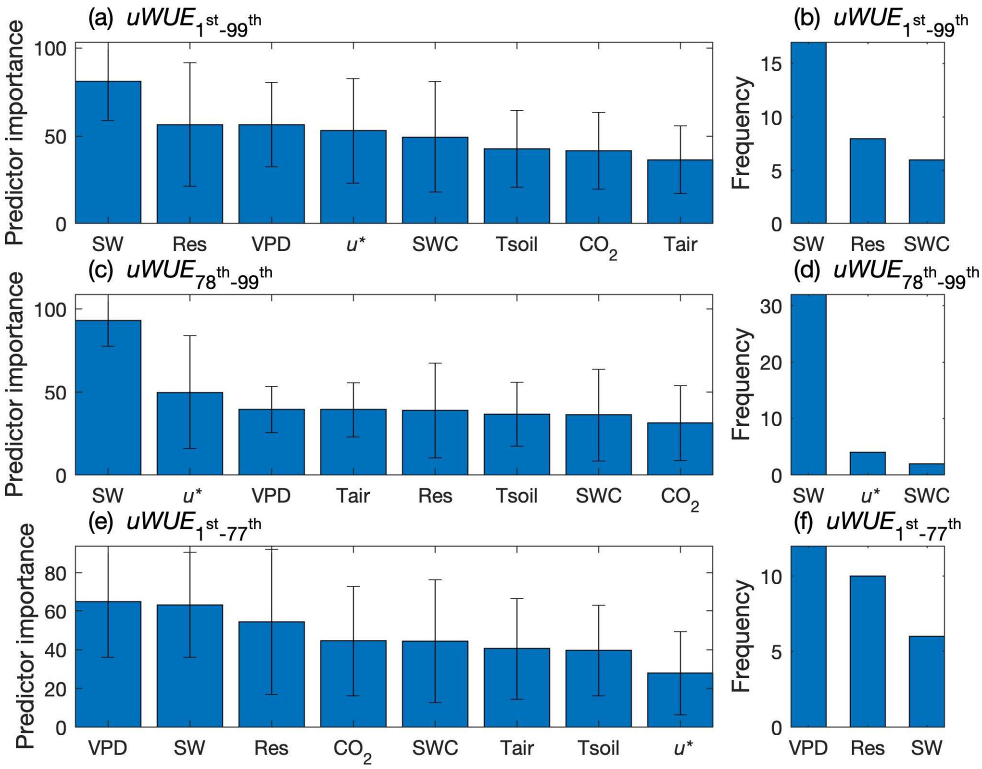

Figure 7. The predictor importance estimated by our random-forest model for the 1st to 99th (a), 78th to 99th (c), and 1st to 77th (e) percentile bins of *uWUE* inferred at individual sites. Blue bars and black error bars represent the mean and standard deviation across

the 40 FLUXNET sites, respectively. Eight climate drivers were compared for their predictor importance on *uWUE*: vapor pressure deficit (VPD), air (Tair) and soil (Tsoil) temperatures, soil water content (SWC), friction velocity (u*), downwelling solar radiation (SW), residual energy imbalance (Res), and atmospheric carbon dioxide concentration (CO_2). The top three frequently identified most important climate drivers controlling the 1^{st} to 99^{th} (b), 78^{th} to 99^{th} (d), and 1^{st} to 77^{th} (f) percentile bins of *uWUE* across the 40 FLUXNET sites.

4. Discussion

Recent observed increases in plant *WUE* have important implications for biosphere-atmosphere interactions under a changing climate, urging reassessment of the ecophysiological parameterization used in existing Earth system models (Adams et al., 2020; Guerrieri et al., 2019; Keenan et al., 2013; Mathias and Thomas, 2021). However, discrepancies between *WUE* trends inferred from different temporal and spatial scales hinder the interpretation and translation to models of the observed ecosystem responses to climate (Knauer et al., 2018; Lavergne et al., 2019; Medlyn et al., 2017). Such discrepancies may stem from indirect CO_2 effects on ecosystem processes (e.g., altering canopy structure and soil moisture (Fatichi et al., 2016)) that modulate the direct CO_2 effects on leaf-scale responses to elevated CO_2 (Lavergne et al., 2019). Additionally, studies often use different data sampling and processing schemes to calculate seasonal *WUE*, even though the same *WUE* functional form is applied. For example, seasonal *WUE* inferred from the same WUE_{ei} definition could be attributed to measurements during May to September (Guerrieri et al., 2019) or June to August

(Keenan et al., 2013), leading to different ecosystem-scale *WUE* trends from observations.

Our analyses indicate that the observed decadal trends in ecosystem-scale *WUE* are controlled primarily by changes in hourly weather conditions (i.e., $uWUE \geq uWUE_{78th}$, labeled here as *MAH*). Temporal variations in *MAH* contribute more to decadal trends in ecosystem-scale *WUE* than those from CO_2 and VPD across the 40 FLUXNET sites. The strong *MAH* effects on decadal *WUE* trends suggests that ecosystem-scale *WUE* cannot be directly compared with those inferred from leaf-scale measurements due to non-ecophysiological factors embedded in measurements taken by the eddy covariance method. For example, canopy structure effects on light competition and turbulent mixing can modulate carbon and water fluxes inferred from eddy covariance measurements, which affects ecosystem-scale *WUE* and contributes to the discrepancies between previously-inferred leaf- and ecosystem- scale *WUE* trends. Consistent results were found using different *WUE* measures (e.g., inherent vs. underlying), data aggregating and processing schemes (e.g., hourly vs. seasonal), and data sampling periods (e.g., growing season vs. summer only, considering wet canopy conditions), buttressing our conclusions regarding the importance of short-term water-carbon interactions on decadal ecosystem-scale *WUE* trends.

Ecosystem-scale water and carbon fluxes inferred from eddy covariance measurements are determined by both leaf-scale ecophysiological strategy (e.g., stomatal responses to microenvironmental conditions varying alone the canopy) and ecosystem-scale eddy mixing (e.g., local and non-local turbulent transport). Therefore, it is important to attribute emergent water-carbon interactions to different drivers to properly interpret ecosystem-scale *WUE* trends and their implications. This conclusion is in line with a recent study showing that causal networks of water-carbon interactions are strongly shaped by prevailing meteorological conditions rather than vegetation type and climatic region (Krich et al., 2021). The large *WUE* sensitivity to hourly weather conditions that we inferred from various approaches may also be relevant to the strong land-air coupling effects that strengthen water-carbon interactions observed at the ecosystem scale (Humphrey et al., 2021; Zhou et al., 2019). Identifying favorable weather conditions leading to higher *WUE* requires dynamically considering interactions among climate and ecophysiological factors, which is not represented in our predictor importance analysis. Measurements of vertically resolved canopy scalar profiles are needed to disentangle factors contributing to emergent water-carbon interactions, as weather conditions measured at the top of the canopy may not accurately represent environmental conditions experienced by plant leaves.

We found large *uWUE* sensitivity to inter-site variability, suggesting that factors controlling the observed *WUE* trends are site-specific (e.g., only species that experienced moisture limitations show reduced stomatal conductance (Guerrieri et al., 2019)). The large *uWUE* sensitivity to solar radiation inferred from hourly timescale demonstrates the importance of short-term ecosystem responses to weather conditions and canopy radiative transfer. Proper representations of canopy structural and functional profiles are thus needed to connect processes underlying water-carbon interactions over a continuum of scales (Bonan et al., 2021; Chang et al., 2018a, 2018b).

Our finding that CMIP6 models did not accurately represent the observed *WUE* sensitivity to inter-site variability and microclimatic conditions further motivates more robust parameterization of water-carbon interactions in the canopy. Ecosystem-scale modeling and observational data synthesis (e.g., Hawkins et al., 2020) that evaluates the land component of Earth system models under a rigorous simulation protocol is needed to identify bottlenecks in representing water-carbon interactions across temporal scales. We recommend future studies distinguish short-term and long-term ecosystem dynamics inferred from eddy covariance measurements to improve interpretation of observed biosphere-atmosphere interactions.

5. Conclusions

Terrestrial plants mitigate anthropogenic climate change by removing a substantial amount of atmospheric carbon dioxide through photosynthesis, a process with unavoidable water loss via transpiration. Water-use efficiency (*WUE*) is a key metric quantifying the amount of carbon gain per unit of water lost, and accurate interpretation of observed *WUE* trends is needed to understand biosphere-atmosphere interactions and improve climate projections. Our results indicate that ecosystem-scale *WUE* trends are strongly modulated by short-term water-carbon interactions associated with hourly weather conditions that typically cover less than 22% of the observational period. Longer-term changes in atmospheric carbon dioxide concentrations and vapor pressure deficit do not individually explain *WUE* trends inferred from the 40 FLUXNET sites. Disentangling the role of microclimatic conditions and long-term trends on ecosystem-scale *WUE* estimates is thus critical to properly translate observationally-inferred ecophysiological understanding into next-generation Earth System Models.

Acknowledgments

This research was supported by the RUBISCO SFA of the Regional and Global Modeling Analysis (RGMA) program in the Climate and Environmental Sciences Division (CESD) of the Biological and Environmental Research (BER) Program in the U.S. Department of Energy Office of Science under contract DE-AC02-05CH11231. TK acknowledges additional support from a NASA Terrestrial Ecology Program IDS Award 80NSSC21K1705. The FLUXNET eddy covariance data processing and harmonization was carried out by the European Fluxes Database Cluster and the AmeriFlux Management Project (with support by European Union H2020 projects and U.S. Department of Energy Office of Science, respectively), with contributions from the Carbon Dioxide Information Analysis Center, ICOS Ecosystem Thematic Centre, and OzFlux, ChinaFlux, and AsiaFlux offices. CarbonTracker CT2019B results provided by NOAA ESRL, Boulder, Colorado, USA from the website at http://carbontracker.noaa.gov.

Data availability

This work used publicly available FLUXNET2015 CC-BY-4.0 Dataset acquired and shared by the FLUXNET community. All related data is publicly available for download at https://fluxnet.org/.

Code availability

Code used in the analysis presented in this study is available online, and can be accessed at https://doi.org/10.5281/zenodo.5140716.

Competing interests

The authors declare no competing interests.

Author Contributions

K.Y.C. and W.J.R. designed the analysis. K.Y.C. processed the data and analyzed the results. All authors contributed extensively to the contents of the manuscript.

References

Adams, M.A., Buckley, T.N., Turnbull, T.L., 2020. Diminishing CO2-driven gains in water-use efficiency of global forests. Nat. Clim. Chang. 10, 1–6. https://doi.org/10.1038/s41558-020-0747-7

Bastos, A., Ciais, P., Friedlingstein, P., Sitch, S., Pongratz, J., Fan, L., Wigneron, J.P., Weber, U., Reichstein, M., Fu, Z., Anthoni, P., Arneth, A., Haverd, V., Jain, A.K., Joetzjer, E., Knauer, J., Lienert, S., Loughran, T., McGuire, P.C., Tian, H., Viovy, N., Zaehle, S., 2020. Direct and seasonal legacy effects of the 2018 heat wave and drought on European ecosystem productivity. Sci. Adv. 6, 1–14. https://doi.org/10.1126/sciadv.aba2724

Bechtold, B., Fletcher, P., Gorur-Shandilya, S., 2021. bastibe/Violinplot-Matlab: A Good Starting Point (v0.1). https://doi.org/10.5281/zenodo.4559847

Beer, C., Ciais, P., Reichstein, M., Baldocchi, D., Law, B.E., Papale, D., Soussana, J.F., Ammann, C., Buchmann, N., Frank, D., Gianelle, D., Janssens, I.A., Knohl, A., Köstner, B., Moors, E., Roupsard, O., Verbeeck, H., Vesala, T., Williams, C.A., Wohlfahrt, G., 2009. Temporal and among-site variability of inherent water use efficiency at the ecosystem level. Global Biogeochem. Cycles 23, 1–13. https://doi.org/10.1029/2008GB003233

Bonan, G.B., Patton, E.G., Finnigan, J.J., Baldocchi, D.D., Harman, I.N., 2021. Moving beyond the incorrect but useful paradigm: reevaluating big-leaf and multilayer plant canopies to model biosphere-atmosphere fluxes – a review. Agric. For. Meteorol. 306, 108435. https://doi.org/10.1016/j.agrformet.2021.108435

Boucher, O., Servonnat, J., Albright, A.L., Aumont, O., Balkanski, Y., Bastrikov, V., Bekki, S., Bonnet, R., Bony, S., Bopp, L., Braconnot, P., Brockmann, P., Cadule, P., Caubel, A., Cheruy, F., Codron, F., Cozic, A., Cugnet, D., D'Andrea, F., Davini, P., de Lavergne, C., Denvil, S., Deshayes, J., Devilliers, M., Ducharne, A., Dufresne, J.-L., Dupont, E., Éthé, C., Fairhead, L., Falletti, L., Flavoni, S., Foujols, M.-A., Gardoll, S., Gastineau, G., Ghattas, J., Grandpeix, J.-Y., Guenet, B., Guez E., L., Guilyardi, E., Guimberteau, M., Hauglustaine, D., Hourdin, F., Idelkadi, A., Joussaume, S., Kageyama, M., Khodri, M., Krinner, G., Lebas, N., Levavasseur, G., Lévy, C., Li, L., Lott, F., Lurton, T., Luyssaert, S., Madec, G., Madeleine, J.-B., Maignan, F., Marchand, M., Marti, O., Mellul, L., Meurdesoif, Y., Mignot, J., Musat, I., Ottlé, C., Peylin, P., Planton, Y., Polcher, J., Rio, C., Rochetin, N., Rousset, C., Sepulchre, P., Sima, A., Swingedouw, D., Thiéblemont, R., Traore, A.K., Vancoppenolle, M., Vial, J., Vialard, J., Viovy, N., Vuichard, N., 2020. Presentation and Evaluation of the IPSL-CM6A-LR Climate Model. J. Adv. Model. Earth Syst. 12, e2019MS002010. https://doi.org/https://doi.org/10.1029/2019MS002010

Burkey, J., 2022. Mann-Kendall Tau-b with Sen's Method (enhanced) [WWW

Document]. MATLAB Cent. File Exch. URL https://www.mathworks.com/matlabcentral/fileexchange/11190-mann-kendall-tau-b-with-sen-s-method-enhanced

Chang, K.-Y., Paw U, K.T., Chen, S.-H., 2018a. The importance of carbon-nitrogen biogeochemistry on water vapor and carbon fluxes as elucidated by a multiple canopy layer higher order closure land surface model. Agric. For. Meteorol. 259, 60–74. https://doi.org/10.1016/j.agrformet.2018.04.009

Chang, K.-Y., Paw U, K.T., Chen, S.-H., 2018b. Canopy profile sensitivity on surface layer simulations evaluated by a multiple canopy layer higher order closure land surface model. Agric. For. Meteorol. 252, 192–207. https://doi.org/10.1016/j.agrformet.2018.01.027

Cherchi, A., Fogli, P.G., Lovato, T., Peano, D., Iovino, D., Gualdi, S., Masina, S., Scoccimarro, E., Materia, S., Bellucci, A., Navarra, A., 2019. Global Mean Climate and Main Patterns of Variability in the CMCC-CM2 Coupled Model. J. Adv. Model. Earth Syst. 11, 185–209. https://doi.org/10.1029/2018MS001369

Danabasoglu, G., Lamarque, J.-F., Bacmeister, J., Bailey, D.A., DuVivier, A.K., Edwards, J., Emmons, L.K., Fasullo, J., Garcia, R., Gettelman, A., Hannay, C., Holland, M.M., Large, W.G., Lauritzen, P.H., Lawrence, D.M., Lenaerts, J.T.M., Lindsay, K., Lipscomb, W.H., Mills, M.J., Neale, R., Oleson, K.W., Otto-Bliesner, B., Phillips, A.S., Sacks, W., Tilmes, S., van Kampenhout, L., Vertenstein, M., Bertini, A., Dennis, J., Deser, C., Fischer, C., Fox-Kemper, B., Kay, J.E., Kinnison, D., Kushner, P.J., Larson, V.E., Long, M.C., Mickelson, S., Moore, J.K., Nienhouse, E., Polvani, L., Rasch, P.J., Strand, W.G., 2020. The Community Earth System Model Version 2 (CESM2). J. Adv. Model. Earth Syst. 12, e2019MS001916. https://doi.org/https://doi.org/10.1029/2019MS001916

Driscoll, A.W., Bitter, N.Q., Sandquist, D.R., Ehleringer, J.R., 2020. Multidecadal records of intrinsic water-use efficiency in the desert shrub Encelia farinosa reveal strong responses to climate change. Proc. Natl. Acad. Sci. U. S. A. 117, 18161–18168. https://doi.org/10.1073/pnas.2008345117

Eyring, V., Bony, S., Meehl, G.A., Senior, C.A., Stevens, B., Stouffer, R.J., Taylor, K.E., 2016. Overview of the Coupled Model Intercomparison Project Phase 6 (CMIP6) experimental design and organization. Geosci. Model Dev. 9, 1937–1958. https://doi.org/10.5194/gmd-9-1937-2016

Fatichi, S., Leuzinger, S., Paschalis, A., Adam Langley, J., Barraclough, A.D., Hovenden, M.J., 2016. Partitioning direct and indirect effects reveals the response of water-limited ecosystems to elevated CO2. Proc. Natl. Acad. Sci. U. S. A. 113, 12757–12762. https://doi.org/10.1073/pnas.1605036113

Friedlingstein, P., O'Sullivan, M., Jones, M.W., Andrew, R.M., Hauck, J., Olsen, A., Peters, G.P., Peters, W., Pongratz, J., Sitch, S., Le Quéré, C., Canadell, J.G., Ciais, P., Jackson, R.B., Alin, S., Aragão, L.E.O.C., Arneth, A., Arora, V., Bates, N.R., Becker, M., Benoit-Cattin, A., Bittig, H.C., Bopp, L., Bultan, S., Chandra, N., Chevallier, F., Chini, L.P., Evans, W., Florentie, L., Forster, P.M., Gasser, T., Gehlen, M., Gilfillan, D., Gkritzalis, T., Gregor, L., Gruber, N., Harris, I., Hartung, K., Haverd, V., Houghton, R.A., Ilyina, T., Jain, A.K., Joetzjer, E., Kadono, K., Kato, E., Kitidis, V., Korsbakken, J.I., Landschützer, P., Lefèvre, N., Lenton, A., Lienert, S., Liu, Z., Lombardozzi, D., Marland, G., Metzl, N., Munro, D.R., Nabel, J.E.M.S., Nakaoka, S.I., Niwa, Y., O'Brien, K., Ono, T., Palmer, P.I., Pierrot, D., Poulter, B., Resplandy, L., Robertson, E., Rödenbeck, C., Schwinger, J., Séférian, R., Skjelvan, I., Smith, A.J.P., Sutton, A.J., Tanhua, T., Tans, P.P., Tian, H., Tilbrook, B., Van Der Werf, G., Vuichard, N., Walker, A.P., Wanninkhof, R., Watson, A.J., Willis, D., Wiltshire, A.J., Yuan, W., Yue, X., Zaehle, S., 2020. Global Carbon Budget 2020. Earth Syst. Sci. Data 12, 3269–3340. https://doi.org/10.5194/essd-12-3269-2020

Guerrieri, R., Belmecheri, S., Ollinger, S. V., Asbjornsen, H., Jennings, K., Xiao, J., Stocker, B.D., Martin, M., Hollinger, D.Y., Bracho-Garrillo, R., Clark, K., Dore, S., Kolb, T., William Munger, J., Novick, K., Richardson, A.D., 2019. Disentangling the role of photosynthesis and stomatal conductance on rising forest water-use efficiency. Proc. Natl. Acad. Sci. U. S. A. 116, 16909–16914. https://doi.org/10.1073/pnas.1905912116

Gutjahr, O., Putrasahan, D., Lohmann, K., Jungclaus, J.H., von Storch, J.-S., Brüggemann, N., Haak, H., Stössel, A., 2019. Max Planck Institute Earth System Model (MPI-ESM1.2) for the High-Resolution Model Intercomparison Project (HighResMIP). Geosci. Model Dev. 12, 3241–3281. https://doi.org/10.5194/gmd-12-3241-2019

Hawkins, L., Kumar, J., Luo, X., Sihi, D., Zhou, S., 2020. Measuring, Monitoring, and Modeling Ecosystem Cycling. Eos (Washington. DC). 101. https://doi.org/10.1029/2020EO147717

Humphrey, V., Berg, A., Ciais, P., Gentine, P., Jung, M., Reichstein, M., Seneviratne, S.I., Frankenberg, C., 2021. Soil moisture – atmosphere feedback dominates land carbon uptake variability. Nature 592. https://doi.org/10.1038/s41586-021-03325-5

Jacobson, A.R., Schuldt, K.N., Miller, J.B., Oda, T., Tans, P., Mund, J., Ott, L., Collatz, G.J., Aalto, T., Afshar, S., Aikin, K., Aoki, S., Apadula, F., Baier, B., Bergamaschi, P., Beyersdorf, A., Biraud, S.C., Bollenbacher, A., Bowling, D., Brailsford, G., Abshire, J.B., Chen, G., 2020. CarbonTracker CT2019B [WWW Document]. https://doi.org/https://doi.org/10.25925/20201008

Keenan, T.F., Hollinger, D.Y., Bohrer, G., Dragoni, D., Munger, J.W., Schmid, H.P., Richardson, A.D., 2013. Increase in forest water-use efficiency as atmospheric carbon dioxide concentrations rise. Nature 499, 324–327. https://doi.org/10.1038/nature12291

Keenan, T.F., Williams, C.A., 2018. The terrestrial carbon sink. Annu. Rev. Environ. Resour. 43, 219–243. https://doi.org/10.1146/annurev-environ-102017-030204

Kelley, M., Schmidt, G.A., Nazarenko, L.S., Bauer, S.E., Ruedy, R., Russell, G.L., Ackerman, A.S., Aleinov, I., Bauer, M., Bleck, R., Canuto, V., Cesana, G., Cheng, Y., Clune, T.L., Cook, B.I., Cruz, C.A., Del Genio, A.D., Elsaesser, G.S., Faluvegi, G., Kiang, N.Y., Kim, D., Lacis, A.A., Leboissetier, A., LeGrande, A.N., Lo, K.K., Marshall, J., Matthews, E.E., McDermid, S., Mezuman, K., Miller, R.L., Murray, L.T., Oinas, V., Orbe, C., García-Pando, C.P., Perlwitz, J.P., Puma, M.J., Rind, D., Romanou, A., Shindell, D.T., Sun, S., Tausnev, N., Tsigaridis, K., Tselioudis, G., Weng, E., Wu, J., Yao, M.-S., 2020. GISS-E2.1: Configurations and Climatology. J. Adv. Model. Earth Syst. 12, e2019MS002025. https://doi.org/https://doi.org/10.1029/2019MS002025

Knauer, J., Zaehle, S., Medlyn, B.E., Reichstein, M., Williams, C.A., Migliavacca, M., De Kauwe, M.G., Werner, C., Keitel, C., Kolari, P., Limousin, J.M., Linderson, M.L., 2018. Towards physiologically meaningful water-use efficiency estimates from eddy covariance data. Glob. Chang. Biol. 24, 694–710. https://doi.org/10.1111/gcb.13893

Knauer, J., Zaehle, S., Reichstein, M., Medlyn, B.E., Forkel, M., Hagemann, S., Werner, C., 2017. The response of ecosystem water-use efficiency to rising atmospheric CO2 concentrations: sensitivity and large-scale biogeochemical implications. New Phytol. 213, 1654–1666. https://doi.org/10.1111/nph.14288

Krich, C., Migliavacca, M., Miralles, D.G., Kraemer, G., El-Madany, T.S., Reichstein, M., Runge, J., Mahecha, M.D., 2021. Functional convergence of biosphere-Atmosphere interactions in response to meteorological conditions. Biogeosciences 18, 2379–2404. https://doi.org/10.5194/bg-18-2379-2021

Lavergne, A., Graven, H., De Kauwe, M.G., Keenan, T.F., Medlyn, B.E., Prentice, I.C., 2019. Observed and modelled historical trends in the water-use efficiency of plants and ecosystems. Glob. Chang. Biol. https://doi.org/10.1111/gcb.14634

Lloyd, J., Shibistova, O., Zolotoukhine, D., Kolle, O., Arneth, A., Wirth, C., Styles, J.M., Tchebakova, N.M., Schulze, E.-D., 2002. Seasonal and annual variations in the photosynthetic productivity and carbon balance of a central Siberian pine forest. Tellus B Chem. Phys. Meteorol. 54, 590–610. https://doi.org/10.3402/tellusb.v54i5.16689

Mastrotheodoros, T., Pappas, C., Molnar, P., Burlando, P., Keenan, T.F., Gentine, P., Gough, C.M., Fatichi, S., 2017. Linking plant functional trait plasticity and the large increase in forest water use efficiency. J. Geophys. Res. Biogeosciences 122, 2393–2408. https://doi.org/10.1002/2017JG003890

Mathias, J.M., Thomas, R.B., 2021. Global tree intrinsic water use efficiency is enhanced by increased atmospheric CO2 and modulated by climate and plant functional types. Proc. Natl. Acad. Sci. U. S. A. 118. https://doi.org/10.1073/pnas.2014286118

Medlyn, B.E., De Kauwe, M.G., Lin, Y.S., Knauer, J., Duursma, R.A., Williams, C.A., Arneth, A., Clement, R., Isaac, P., Limousin, J.M., Linderson, M.L., Meir, P., Martin-Stpaul, N., Wingate, L., 2017. How do leaf and ecosystem measures of water-use efficiency compare? New Phytol. https://doi.org/10.1111/nph.14626

Nelson, J.A., Pérez-Priego, O., Zhou, S., Poyatos, R., Zhang, Y., Blanken, P.D., Gimeno, T.E., Wohlfahrt, G., Desai, A.R., Gioli, B., Limousin, J.M., Bonal, D., Paul-Limoges, E., Scott, R.L., Varlagin, A., Fuchs, K., Montagnani, L., Wolf, S., Delpierre, N., Berveiller, D., Gharun, M., Belelli Marchesini, L., Gianelle, D., Šigut, L., Mammarella, I., Siebicke, L., Andrew Black, T., Knohl, A., Hörtnagl, L., Magliulo, V., Besnard, S., Weber, U., Carvalhais, N., Migliavacca, M., Reichstein, M., Jung, M., 2020. Ecosystem transpiration and evaporation: Insights from three water flux partitioning methods across FLUXNET sites. Glob. Chang. Biol. 26, 6916–6930. https://doi.org/10.1111/gcb.15314

Pastorello, G., Trotta, C., Canfora, E., Chu, H., Christianson, D., Cheah, Y.-W., Poindexter, C., Chen, J., Elbashandy, A., Humphrey, M., Isaac, P., Polidori, D., Ribeca, A., van

Ingen, C., Zhang, L., Amiro, B., Ammann, C., Arain, M.A., Ardö, J., Arkebauer, T., Arndt, S.K., Arriga, N., Aubinet, M., Aurela, M., Baldocchi, D., Barr, A., Beamesderfer, E., Marchesini, L.B., Bergeron, O., Beringer, J., Bernhofer, C., Berveiller, D., Billesbach, D., Black, T.A., Blanken, P.D., Bohrer, G., Boike, J., Bolstad, P. V., Bonal, D., Bonnefond, J.-M., Bowling, D.R., Bracho, R., Brodeur, J., Brümmer, C., Buchmann, N., Burban, B., Burns, S.P., Buysse, P., Cale, P., Cavagna, M., Cellier, P., Chen, S., Chini, I., Christensen, T.R., Cleverly, J., Collalti, A., Consalvo, C., Cook, B.D., Cook, D., Coursolle, C., Cremonese, E., Curtis, P.S., D’Andrea, E., da Rocha, H., Dai, X., Davis, K.J., De Cinti, B., de Grandcourt, A., De Ligne, A., De Oliveira, R.C., Delpierre, N., Desai, A.R., Di Bella, C.M., di Tommasi, P., Dolman, H., Domingo, F., Dong, G., Dore, S., Duce, P., Dufrêne, E., Dunn, A., Dušek, J., Eamus, D., Eichelmann, U., ElKhidir, H.A.M., Eugster, W., Ewenz, C.M., Ewers, B., Famulari, D., Fares, S., Feigenwinter, I., Feitz, A., Fensholt, R., Filippa, G., Fischer, M., Frank, J., Galvagno, M., Gharun, M., Gianelle, D., Gielen, B., Gioli, B., Gitelson, A., Goded, I., Goeckede, M., Goldstein, A.H., Gough, C.M., Goulden, M.L., Graf, A., Griebel, A., Gruening, C., Grünwald, T., Hammerle, A., Han, S., Han, X., Hansen, B.U., Hanson, C., Hatakka, J., He, Y., Hehn, M., Heinesch, B., Hinko-Najera, N., Hörtnagl, L., Hutley, L., Ibrom, A., Ikawa, H., Jackowicz-Korczynski, M., Janouš, D., Jans, W., Jassal, R., Jiang, S., Kato, T., Khomik, M., Klatt, J., Knohl, A., Knox, S., Kobayashi, H., Koerber, G., Kolle, O., Kosugi, Y., Kotani, A., Kowalski, A., Kruijt, B., Kurbatova, J., Kutsch, W.L., Kwon, H., Launiainen, S., Laurila, T., Law, B., Leuning, R., Li, Yingnian, Liddell, M., Limousin, J.-M., Lion, M., Liska, A.J., Lohila, A., López-Ballesteros, A., López-Blanco, E., Loubet, B., Loustau, D., Lucas-Moffat, A., Lüers, J., Ma, S., Macfarlane, C., Magliulo, V., Maier, R., Mammarella, I., Manca, G., Marcolla, B., Margolis, H.A., Marras, S., Massman, W., Mastepanov, M., Matamala, R., Matthes, J.H., Mazzenga, F., McCaughey, H., McHugh, I., McMillan, A.M.S., Merbold, L., Meyer, W., Meyers, T., Miller, S.D., Minerbi, S., Moderow, U., Monson, R.K., Montagnani, L., Moore, C.E., Moors, E., Moreaux, V., Moureaux, C., Munger, J.W., Nakai, T., Neirynck, J., Nesic, Z., Nicolini, G., Noormets, A., Northwood, M., Nosetto, M., Nouvellon, Y., Novick, K., Oechel, W., Olesen, J.E., Ourcival, J.-M., Papuga, S.A., Parmentier, F.-J., Paul-Limoges, E., Pavelka, M., Peichl, M., Pendall, E., Phillips, R.P., Pilegaard, K., Pirk, N., Posse, G., Powell, T., Prasse, H., Prober, S.M., Rambal, S., Rannik, Ü., Raz-Yaseef, N., Reed, D., de Dios, V.R., Restrepo-Coupe, N., Reverter, B.R., Roland, M., Sabbatini, S., Sachs, T., Saleska, S.R., Sánchez-Cañete, E.P., Sanchez-Mejia, Z.M., Schmid, H.P., Schmidt, M., Schneider, K., Schrader, F., Schroder, I., Scott, R.L., Sedlák, P., Serrano-Ortíz, P., Shao, C., Shi, P., Shironya, I., Siebicke, L., Šigut, L., Silberstein, R., Sirca, C., Spano, D., Steinbrecher, R., Stevens, R.M., Sturtevant, C., Suyker, A., Tagesson, T., Takanashi, S., Tang, Y., Tapper, N., Thom, J., Tiedemann, F., Tomassucci, M., Tuovinen, J.-P., Urbanski, S., Valentini, R., van der Molen, M., van Gorsel, E., van Huissteden, K., Varlagin, A., Verfaillie, J., Vesala, T., Vincke, C., Vitale, D., Vygodskaya, N., Walker, J.P., Walter-Shea, E., Wang, H., Weber, R., Westermann, S., Wille, C., Wofsy, S., Wohlfahrt, G., Wolf, S., Woodgate, W., Li, Yuelin, Zampedri, R., Zhang, J., Zhou, G., Zona, D., Agarwal, D., Biraud, S., Torn, M., Papale, D., 2020. The FLUXNET2015 dataset and the ONEFlux processing pipeline for eddy covariance data. Sci. Data 7, 225. https://doi.org/10.1038/s41597-020-0534-3

Reich, P.B., Hobbie, S.E., Lee, T.D., Rich, R., Pastore, M.A., Worm, K., 2020. Synergistic effects of four climate change drivers on terrestrial carbon cycling. Nat. Geosci. 13, 787–793. https://doi.org/10.1038/s41561-020-00657-1

Schulze, E.-D., Hall, A.E., 1982. Stomatal Responses, Water Loss and CO2 Assimilation Rates of Plants in Contrasting Environments, in: Lange, O.L., Nobel, P.S., Osmond, C.B., Ziegler, H. (Eds.), Physiological Plant Ecology II: Water Relations and Carbon Assimilation. Springer Berlin Heidelberg, Berlin, Heidelberg, pp. 181–230. https://doi.org/10.1007/978-3-642-68150-9_8

Seland, Ø., Bentsen, M., Olivié, D., Toniazzo, T., Gjermundsen, A., Graff, L.S., Debernard, J.B., Gupta, A.K., He, Y.-C., Kirkevåg, A., Schwinger, J., Tjiputra, J., Aas, K.S., Bethke, I., Fan, Y., Griesfeller, J., Grini, A., Guo, C., Ilicak, M., Karset, I.H.H., Landgren, O., Liakka, J., Moseid, K.O., Nummelin, A., Spensberger, C., Tang, H., Zhang, Z., Heinze, C., Iversen, T., Schulz, M., 2020. Overview of the Norwegian Earth System Model (NorESM2) and key climate response of CMIP6 DECK, historical, and scenario simulations. Geosci. Model Dev. 13, 6165–6200. https://doi.org/10.5194/gmd-13-6165-2020

Swart, N.C., Cole, J.N.S., Kharin, V. V., Lazare, M., Scinocca, J.F., Gillett, N.P., Anstey, J., Arora, V., Christian, J.R., Hanna, S., Jiao, Y., Lee, W.G., Majaess, F., Saenko, O.A., Seiler, C., Seinen, C., Shao, A., Sigmond, M., Solheim, L., Von Salzen, K., Yang, D., Winter, B., 2019. The Canadian Earth System Model version 5 (CanESM5.0.3). Geosci. Model Dev. 12, 4823–4873. https://doi.org/10.5194/gmd-12-4823-2019

Ueyama, M., Ichii, K., Kobayashi, H., Kumagai, T., Beringer, J., Merbold, L., Euskirchen, E.S., Hirano, T., Marchesini, L.B., Baldocchi, D., Saitoh, T.M., Mizoguchi, Y., Ono, K., Kim, J., Varlagin, A., Kang, M., Shimizu, T., Kosugi, Y., Bret-Harte, M.S., MacHimura, T., Matsuura, Y., Ohta, T., Takagi, K., Takanashi, S., Yasuda, Y., 2020. Inferring CO_2fertilization effect based on global monitoring land-atmosphere exchange with a theoretical model. Environ. Res. Lett. 15. https://doi.org/10.1088/1748-9326/ab79e5

Walker, A.P., De Kauwe, M.G., Bastos, A., Belmecheri, S., Georgiou, K., Keeling, R.F., McMahon, S.M., Medlyn, B.E., Moore, D.J.P., Norby, R.J., Zaehle, S., Anderson‐Teixeira, K.J., Battipaglia, G., Brienen, R.J.W., Cabugao, K.G., Cailleret, M., Campbell, E., Canadell, J.G., Ciais, P., Craig, M.E., Ellsworth, D.S., Farquhar, G.D., Fatichi, S., Fisher, J.B., Frank, D.C., Graven, H., Gu, L., Haverd, V., Heilman, K., Heimann, M., Hungate, B.A., Iversen, C.M., Joos, F., Jiang, M., Keenan, T.F., Knauer, J., Körner, C., Leshyk, V.O., Leuzinger, S., Liu, Y., MacBean, N., Malhi, Y., McVicar, T.R., Penuelas, J., Pongratz, J., Powell, A.S., Riutta, T., Sabot, M.E.B., Schleucher, J., Sitch, S., Smith, W.K., Sulman, B., Taylor, B., Terrer, C., Torn, M.S., Treseder, K.K., Trugman, A.T., Trumbore, S.E., Mantgem, P.J., Voelker, S.L., Whelan, M.E., Zuidema, P.A., 2020. Integrating the evidence for a terrestrial carbon sink caused by increasing atmospheric CO_2. New Phytol. nph.16866. https://doi.org/10.1111/nph.16866

Wohlfahrt, G., Haslwanter, A., Hörtnagl, L., Jasoni, R.L., Fenstermaker, L.F., Arnone, J.A., Hammerle, A., 2009. On the consequences of the energy imbalance for calculating surface conductance to water vapour. Agric. For. Meteorol. 149, 1556–1559.

https://doi.org/10.1016/j.agrformet.2009.03.015
Yi, K., Maxwell, J.T., Wenzel, M.K., Roman, D.T., Sauer, P.E., Phillips, R.P., Novick, K.A., 2019. Linking variation in intrinsic water-use efficiency to isohydricity: a comparison at multiple spatiotemporal scales. New Phytol. 221, 195–208. https://doi.org/10.1111/nph.15384
Zhou, S., Park Williams, A., Berg, A.M., Cook, B.I., Zhang, Y., Hagemann, S., Lorenz, R., Seneviratne, S.I., Gentine, P., 2019. Land–atmosphere feedbacks exacerbate concurrent soil drought and atmospheric aridity. Proc. Natl. Acad. Sci. U. S. A. 116, 18848–18853. https://doi.org/10.1073/pnas.1904955116
Zhou, S., Yu, B., Huang, Y., Wang, G., 2014. The effect of vapor pressure deficit on water use efficiency at the subdaily time scale. Geophys. Res. Lett. https://doi.org/10.1002/2014GL060741
Zscheischler, J., Fatichi, S., Wolf, S., Blanken, P.D., Bohrer, G., Clark, K., Desai, A.R., Hollinger, D., Keenan, T., Novick, K.A., Seneviratne, S.I., 2016. Short-term favorable weather conditions are an important control of interannual variability in carbon and water fluxes. J. Geophys. Res. Biogeosciences 121, 2186–2198. https://doi.org/10.1002/2016JG003503